Theoretical and Applied Fracture Mechanics 122 (2022) 103641

Contents lists available at ScienceDirect

Theoretical and Applied Fracture Mechanics

journal homepage: www.elsevier.com/locate/tafmec

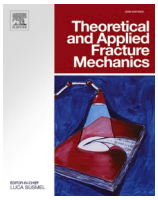

A non-linear cohesive zone model for low-cycle fatigue of quasi-brittle materials

Xun Xi [a,b], Shangtong Yang [b,*]

[a] School of Civil and Resource Engineering, University of Science and Technology Beijing, Beijing 100083, China
[b] Department of Civil and Environmental Engineering, University of Strathclyde, Glasgow G1 1XJ, UK

ARTICLE INFO

Keywords:
Cohesive zone model
Low-cycle fatigue
Nonlinear fatigue damage
Quasi-brittle materials
S–N curve

ABSTRACT

The low-cycle fatigue behaviour of quasi-brittle materials (e.g., concrete and rock) that is characterized by fatigue induced inelastic deformation significantly affects the integrity and serviceability of engineering structures. However, the low-cycle fatigue mechanism and fatigue-controlled fracture process of quasi-brittle materials is not clear. This paper develops a new cyclic cohesive zone model (CZM) for low-cycle fatigue of quasi-brittle materials. Based on in-situ stress and damage state, a nonlinear fatigue damage model is proposed and implemented into the cyclic CZM. The fatigue parameters are determined based on S–N curve. A worked example for monotonic and cyclic loading of concrete beam under three-point bending is presented to demonstrate the application of the developed numerical model. After validation against experimental data, the fatigue crack mechanisms are discussed and a comprehensive parametric study is carried out to investigate the effects of fatigue parameters, stress levels and loading sequences on the fatigue failure. It has been found that there are three stages for the development of crack mouth of displacement, i.e., crack initiation, stable growth and rapid fracture which are caused by combined static and fatigue damage, fatigue damage, and combined static and fatigue damage dominated by static damage, respectively. The developed cyclic CZM is practically significant and its parameters are easy to be determined based on S–N curve. It provides a new and useful tool for low-cycle fatigue crack modelling of quasi-brittle materials.

1. Introduction

Quasi-brittle materials including concrete, rock and ceramics, etc., are characterized by the presence of a fracture process zone with non-negligible size ahead of the crack tip [1,2]. The fracture of quasi-brittle materials is crucial for many engineering applications, e.g., structural durability and integrity, rock slope stability, hydraulic fracking, etc. The monotonic fracture responses of quasi-brittle materials have been well understood and documented. However, the fatigue mechanism and fatigue controlled fracture process of quasi-brittle materials have been less researched. For instance, concrete bridges are often subjected to cyclic loads from wind and wave effects to earthquake- and traffic-induced wave propagation; from the material point of view, the mechanical properties of concrete are degraded and the degradation is dependent on the characteristics of the cyclic loads. Moreover, comparing to high-cycle fatigue, low-cycle fatigue usually generates inelastic deformation after every cycle which significantly affects the serviceability and safety of engineering structures [3–5]. In particular, some new techniques have been developed to stimulate low-cycle fatigue of rock to extract geo-energy, e.g., pulsating fracking [6,7], cyclic-thermal drilling [8,9], etc. Therefore, understanding the low-cycle fatigue fracture of quasi-brittle materials is highly desired for the anti-fatigue design of engineering structures and optimization of fatigue-assistant cracking activities.

The S–N curve (load versus number of cycles to failure) is perhaps the most common and traditional tool for fatigue life assessment [10–12]. Through the S–N curve determined from cyclic loading tests at different constant stress levels, the remaining life or limiting stress for the desired structural life can be obtained. The S–N curve for the fracture of quasi-brittle materials can be obtained by the direct tensile test [4], three-point bending beam test [13], Brazilian disc test [14], etc. Although the experimentally established S–N curve is practical to be used for fatigue life assessment, it is insufficient to understand the fatigue fracture behaviour of quasi-brittle materials due to: (1) the S–N curve only predicts the overall fatigue life of the materials while it does not consider the in-situ fatigue damage and crack propagation and; (2) the fracture of

* Corresponding author.
E-mail address: shangtong.yang@strath.ac.uk (S. Yang).

https://doi.org/10.1016/j.tafmec.2022.103641
Received 25 April 2022; Received in revised form 13 October 2022; Accepted 14 October 2022
Available online 19 October 2022

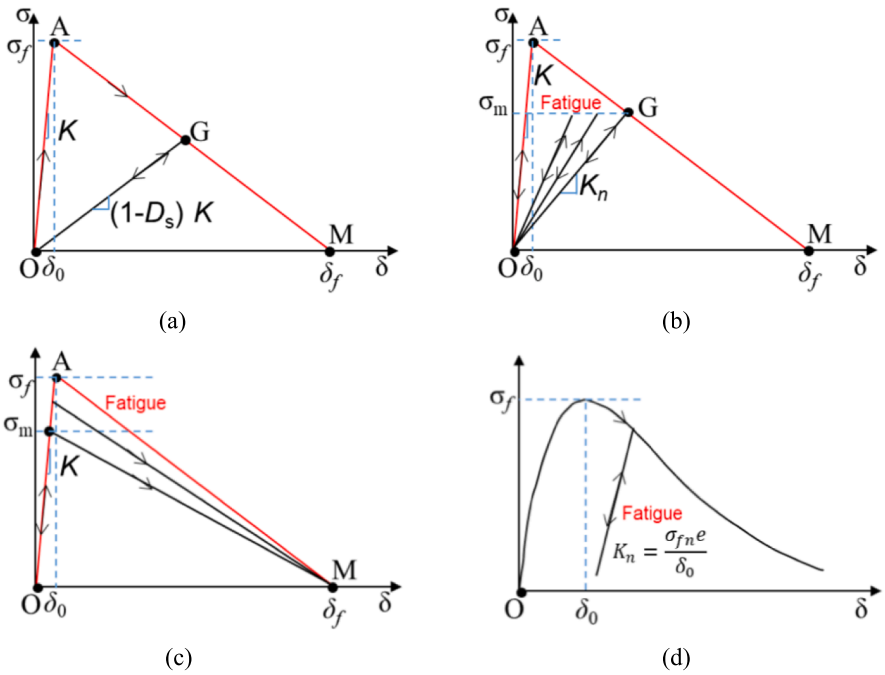

Fig. 1. Illustrations of monotonic and cyclic cohesive zone models: (a) monotonic CZM [19,54,55]; (b) cyclic CZM by stiffness degradation [7,33,56]; (c) cyclic CZM by strength degradation [29,30,45,57]; (d) cyclic CZM by both strength and stiffness degradation [35,58,59].

tested specimen under constant loading amplitudes is unstable and it does not include the post-peak softening behaviour for the quasi-brittle materials.

To predict the fatigue crack growth, Paris law is a widely accepted method which defines the crack extension per incremental number of cycles as a function of the range of stress intensity factor [15,16]. The fatigue crack propagation is normally divided into three stages: crack initiation (short cracks), stable propagation (long cracks) and fast crack propagation (final fracture) [15]. Paris law is supposed to model the stable propagation stage (60–80% of the entire fatigue life) for fatigue crack propagation [17]. Moreover, Paris law is based on the linear elastic fracture mechanics thus it can only be used for specimens with an initial crack for the determination of stress intensity factor. However, fracture in quasi-brittle materials is characterized by distributed post-peak softening damage within the fracture process zone (FPZ) where fatigue crack growth interacts with the progressive damage [18]. Therefore, theoretical justifications of Paris law for quasi-brittle materials are required.

Since Hillerborg et al. [19] first proposed the cohesive model to simulate discrete cracking in the FPZ of concrete, the cohesive zone model (CZM) has been widely employed to model the cracking of composites, rock, and coal given the same quasi-brittle nature [20–26]. Fig. 1a illustrates the relationship between the traction stress and separation displacement for a typical monotonic cohesive law. There are three basic parameters in the monotonic cohesive law, i.e., penalty stiffness which should be significantly larger than the material stiffness to ensure that there is almost no deformation of the fictitious crack before crack initiation; cohesive strength which is the fracture strength of materials; fracture energy which is the energy required to make a unit area of a fracture surface complete separation (the area of OAM). The cohesive stress first linearly increases until the peak stress and then gradually decreases while the stiffness softens. The softening curve can be linear, bi-linear, exponential or other forms [27]. If unloading occurs during the softening, the stress will decrease by a slope of a damaged stiffness and return to the origin. It is clear that the monotonic cohesive law is not able to model the fatigue cracking because a fatigue load smaller than the cohesive strength will only cause repetitive linear elastic deformation.

With the success of CZM in modelling the fracture of quasi-brittle materials, it would be ideal to extend the capability of CZM to fatigue crack growth simulation. A key to develop a cyclic CZM is to introduce a fatigue damage variable into the constitutive model. A common approach for developing cyclic CZMs is to directly employ a cycle-dependent degradation of strength or stiffness in the constitutive formulation (see Fig. 1c-d). Yang et al. [28] first proposed a cyclic CZM for fatigue crack growth in quasi-brittle materials and introduced a reduction of unloading stiffness for the unloading back to the origin. Through the degradation of stiffness, the fatigue damage at loading–unloading cycles below the monotonic envelope were accumulated and thus the simulation of fatigue crack growth became possible. Roth et al. [29,30] developed a cyclic CZM and proposed a concept of cohesive zone potential to determine the stiffness degradation. However, in these cyclic CZMs based on stiffness degradation, the fatigue damage was accumulated after the first cycle so the crack initiation was not explicitly considered [17]. Khoramishad et al.[31–33] believed the fatigue-induced strength degradation should dominate in fatigue crack growth and developed a cyclic CZM based on strength degradation. Xi et al. [7] developed a cyclic CZM coupled with fluid flowing and considered fatigue-induced strength degradation for crack initiation. Nojavan et al.[17] proposed a cyclic CZM for unified crack initiation and propagation, in which the strength degradation determined the crack initiation and stiffness degradation determined the crack propagation. Benedetti and Gulizzi [34] developed a three-dimensional cohesive zone model for inter-granular high-cycle fatigue degradation in polycrystals and implemented it into boundary element method.

However, the above cyclic CZM models all assume that the unloading path returns back to the origin, i.e., zero deformation, which is not true for low-cycle fatigue of quasi-brittle materials. Chen et al. [4] carried out the direct tensile tests of concrete under high stress levels (0.8–0.95 time of monotonic strength) and found that a significant portion of irreversible displacement or inelastic deformation existed per loading cycle. To account for the irreversible displacement, Roe and Siegmund [35] proposed a cyclic CZM for interface fatigue crack growth simulation (see Fig. 1d). The Roe-Siegmund model is based on Needleman monotonic

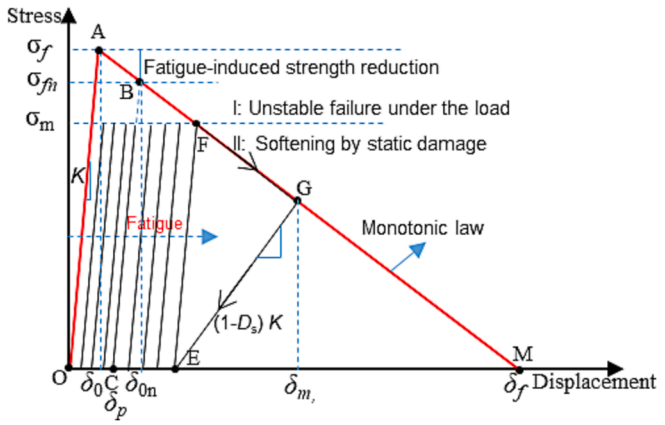

Fig. 2. Cohesive law for low-cycle fatigue of quasi-brittle materials.

CZM which describes the traction-separation law by an ingenious exponential function [35]. However, the Needleman CZM is not a general CZM because it only contains two fatigue parameters, i.e., strength and the critical displacement to the strength, which enlarges the unrealistic deformation before crack initiation [36]. Furthermore, the fatigue damage variable in the Roe-Siegmund cyclic CZM simultaneously reduces the strength and stiffness [35]. Skar et al. [37,38] developed a cyclic CZM in which different stiffness values for unloading and reloading were considered for fatigue damage and a fixed negative intersecting point below the origin on the stress axis was assumed for irreversible deformation. Parrinello and Benedetti [39] developed an elastic–plastic cohesive laws for polycrystalline low-cycle fatigue and the cohesive-frictional behaviour can be considered [40]. Their models [39,40] were formulated in a thermodynamically consistent framework and based on plasticity and damage mechanics with non-associative flow rule for damage evolution.

Another key issue for cyclic CZMs is the determination of fatigue damage evolution. Miner proposed a linear fatigue damage model based on S–N curve in 1954 [41]. Due to its simplicity and ease of application for Miner's model, it is still widely used in the fatigue design of structures [42] and cyclic CZMs [7,17,31–33]. However, the linear fatigue damage model [41] assumes the same fatigue damage increment per cycle under a constant amplitude, which cannot be true because, as the residual strength is gradually decreased, the fatigue damage should be accumulated in an accelerated manner, given the same loading amplitude. Moreover, the effect of loading sequence on the fatigue damage under varying amplitude loads is not considered in the linear fatigue damage model [42]. Further, some nonlinear fatigue damage models were proposed by introducing a power variable to Miner's model [42,43]. Based on the revised Miner's models, the fatigue damage should transfer from one stress level to another for the prediction of residual life under loading with varying amplitudes [42], which brings inconvenience to be used in cyclic CZMs. The fatigue damage can also be determined by Paris law [15,17,44]. However, Paris law based CZM introduces some ambiguities because Paris law is associated with a mathematically sharp, point-wise crack-tip according to the definition based on LEFM, while CZM represents a nonlinear fracture process zone with finite size [17,45]. The literature review suggests (1) there is a lack of general cyclic cohesive zone model considering irreversible deformation for low-cycle fatigue of quasi-brittle materials; (2) there is a research gap for developing a nonlinear fatigue damage model and implementing it into the cyclic CZM. Therefore, it is well justified that a new cyclic CZM be developed to model the nonlinear fatigue damage accumulation and crack growth for low-cycle fatigue of quasi-brittle materials.

This paper develops a cyclic cohesive zone model for low-cycle fatigue of quasi-brittle materials. The cyclic fatigue model is based on a general bilinear monotonic CZM. The low-cycle fatigue induced irreversible displacement is considered in the cyclic CZM. The fatigue and static damage variables are used for irreversible displacement accumulation and stiffness degradation, respectively. A nonlinear fatigue damage model is proposed to calculate the fatigue damage in the cyclic CZM. The fatigue damage parameters are determined based only on experimental S–N data and the fatigue damage evolution derived from the fatigue model is compared with that from experimental results. Further, the developed cyclic CZM is implemented into ABAQUS solver by a VUMAT subroutine. To demonstrate the application of the developed numerical method, a worked example for monotonic and cyclic loading of three-point bending concrete beam is presented. Moreover, the fatigue crack mechanisms are discussed through analysing the stress and damage distributions and evolutions along the potential cracking path. Finally, a comprehensive parametric study is carried out to investigate the effects of fatigue parameters, stress levels and loading sequences on the fatigue failure.

2. New cyclic cohesive zone model

The new cyclic cohesive zone model consists of two regimes. First, it includes the monotonic cohesive laws for static fracture. In this paper, a typical CZM with linear softening is introduced [46,47]. Fig. 1a illustrates the traction-separation law (i.e., stress-displacement relationship) for static Mode I fracture of quasi-brittle materials. The stress is a function of the corresponding relative displacements of the crack surface. For a cohesive crack, the stress will linearly increase to the cohesive strength by a penalty stiffness and then gradually decrease to zero stress. The stress–displacement relationship in the linear elastic stage can be expressed as follows:

$$\sigma = K\delta \tag{1}$$

where σ and δ are the cohesive stress and crack opening displacement, respectively; K is the penalty stiffness.

It is worthwhile to mention that the cohesive crack is a fictitious crack thus there should not be significant separation or displacement before cracking. Therefore, the penalty stiffness must be large enough to hold the two surfaces of the bulk concrete together prior to crack initiation, leading to the same performance as that of no interface existing [48]. However, the penalty stiffness cannot be infinitely large because it will cause convergence problems and increase the computational cost [27]. In this study, the penalty stiffness is set as 10,000 GPa which is approximately 300 times of the bulk materials.

After reaching the strength, the tensile stress gradually decreases following certain softening rules. A linear softening curve is considered in this study for simplification. The residual stress of the cohesive element can be expressed as follows:

$$\sigma = (1 - D_s)K\delta \tag{2}$$

where D_s is the static damage parameter.

It can be seen that the static damage reduces the penalty stiffness from K to $(1-D_s)K$. If unloading occurs at point G (in Fig. 1a), the unloading stiffness is also $(1-D_s)K$ and the curve will return the origin, i.e., zero deformation. Thus, the static damage only regulates the stiffness, which can be determined as follows [21]:

$$D_s = \frac{\delta_f(\delta_m - \delta_0)}{\delta_m\left(\delta_f - \delta_0\right)} \tag{3}$$

where δ_0 is the critical displacement to the cohesive strength (i.e., $D_s = 0$); δ_m is the historical maximum displacement during the loading history; δ_f is the failure displacement when the stress reduces to zero (i.e., D_s=1);

The fracture energy G_f is the area under the stress-displacement curve (i.e., triangle OAM in Fig. 1a). The fracture energy can thus be calculated as follows:

$$G_f = \frac{K\delta_0\delta_f}{2} \tag{4}$$

According to numerous experimental results [4,5,13,35], the monotonic CZM will be extended to a cyclic CZM for low-cycle fatigue of quasi-brittle materials with the following assumptions: (1) irreversible deformation before failure for low-cycle fatigue is significant. (2) the fatigue damage has little effect on the increasing slope of stress (i.e., stiffness) before fatigue failure. (3) the monotonic CZM is the envelope curve of the cyclic CZM, i.e., fatigue won't enhance the mechanical properties of quasi-brittle materials. In this model, fatigue causes the accumulation of irreversible displacement while the static damage causes stiffness degradation. Fig. 2 illustrates the stress-displacement relationship for the cyclic CZM. Under cyclic loading with the maximum stress amplitude σ_m which is smaller than the static strength σ_f, the fatigue damage parameter D_f and the irreversible displacement δ_p will develop. We define the fatigue damage for quasi-brittle materials as follows:

$$D_f = \frac{\delta_p}{\delta_f} \tag{5}$$

D_f is 0 for the first cycle and 1 for irreversible displacement reaching the monotonic failure displacement δ_f. After n cycles (point C in Fig. 2), the residual strength becomes σ_{fn}. The triangles OAM and CBM are similar triangles due to the same penalty stiffness K. It is thus easy to obtain the relationship below:

$$\frac{\sigma_{fn}}{\sigma_f} = \frac{\delta_f - \delta_p}{\delta_f} \tag{6}$$

Accordingly, the relationship between fatigue damage and residual strength can be expressed as follows:

$$\sigma_{fn} = (1 - D_f)\sigma_f \tag{7}$$

Therefore, the fatigue damage can also be regarded as the strength degradation due to inelastic displacement. The area of the translation curve (i.e., OCBA) is the fatigue-induced energy dissipation. Further, the critical displacement to the residual strength can be expressed as follows:

$$\delta_{0n} = (1 - D_f)\delta_0 \tag{8}$$

Before the residual strength reduces to the maximum cyclic loading amplitude (for instance, point F in Fig. 2), the stress-displacement relationship can be calculated as follows:

$$\sigma = K(\delta - \delta_p) \tag{9}$$

Substituting Eq. (5) into Eq. (9), the stress-displacement relationship can be obtained as follows:

$$\sigma = K(\delta - D_f\delta_f) \tag{10}$$

If the fatigue damage is known, the fatigue behaviour before the maximum loading amplitude reaching the residual strength can be determined by Eq. (9). Once the strength is degraded to the maximum load (e.g., point F in Fig. 2), two potential cracking scenarios may happen in the next loading cycle: (1) if the in-situ maximum stress keeps the same, the maximum stress will exceed the residual strength and unstable failure will occur; (2) for stable cracking, the stress will reduces following the softening curve and static damage will occur. In the new updated CZM (triangle EFM in Fig. 2), the static damage can be expressed as follows:

$$D_s = \frac{(\delta_f - \delta_p)(\delta_m - \delta_p - \delta_{0n})}{(\delta_m - \delta_p)(\delta_f - \delta_p - \delta_{0n})} \tag{11}$$

The historical maximum displacement δ_m represents the maximum static damage. δ_m can be expressed as follows:

$$\delta_m = \frac{(\delta_f - \delta_p)\delta_{0n}}{(\delta_f - \delta_p) - D_s[\delta_f - \delta_p - \delta_{0n}]} + \delta_p \tag{12}$$

If the next displacement continues larger than δ_m, static damage will increase. Otherwise, fatigue damage will continue to accumulate under the updated softening curve. Finally, the stress-displacement relationship for coupled fatigue and static damage can be derived as follows:

$$\sigma = \begin{cases} K\delta & \delta < 0 \\ 0 & 0 \le \delta \le D_f\delta_f \\ (1 - D_s)K(\delta - D_f\delta_f) & \delta > D_f\delta_f \end{cases} \tag{13}$$

where $\delta < 0$ means the compressive state; $\delta \le D_f\delta_f$ means the irreversible deformation.

Through Eqs. (5), (11) and (13), the stress-displacement relationship for the new cyclic CZM is established. The new cyclic CZM uses fatigue damage to account for irreversible displacement and static damage for stiffness degradation. In the developed cyclic CZM, the energy balances are ensured during all loading cycles by accounting for fatigue and static damage. If the maximum load in a cycle is lower than the strength, the mechanical energy dissipation can be calculated by the fatigue-induced strength reduction and irreversible displacement (e.g., OABC in Fig. 2). While the maximum load in a cycle is higher than the strength, the mechanical energy dissipation is calculated by the stiffness softening (e.g., EFG in Fig. 2).

3. Nonlinear fatigue damage model

A S–N curve based fatigue damage model is developed. Miner proposed a linear fatigue damage model based on S–N curve in 1954 [41], which can be expressed as follows:

$$D_{fn} = \frac{n_i}{N_f} \tag{14}$$

where D_{fn} is the fatigue damage at the cycle number n_i with a constant fatigue amplitude; N_f is the number of cycle to failure.

Based on Miner's model, the sum of damage fractions for varying loading amplitudes is 1. In fact, the fatigue damage evolution should not be linear while the fatigue damage is progressively accumulated and the residual strength is gradually decreased. To overcome this shortcoming of Miner's rule, some nonlinear fatigue damage models were proposed by introducing a power variable to Miner's model:

$$D_{fn} = 1 - \left(1 - \frac{n_i}{N_f}\right)^{\varphi} \tag{15}$$

where $\varphi = 1$ for Miner's model [41]; φ is a material constant in [43,49]; $\varphi = -1.25/\ln N_f$ in [42].

The nonlinear fatigue models can be used for varying amplitude loading through damage transfer from different stress level and experienced fatigue cycles. However, the damage transfer is complex and difficult to be used in the numerical algorithm because the in-situ cyclic stress is always varying with the fatigue crack growth. Therefore, a nonlinear fatigue damage model based on cyclic stress and in-situ damage state is needed.

3.1. Heuristic fatigue damage model

For each cycle, it is reasonable to assume the fatigue damage increment is a function of the in-situ residual strength and maximum cyclic stress, which can be expressed as follows:

$$\frac{dD_f}{dN} = f\left(\frac{\sigma_{max}}{\sigma_{fn}}\right) \tag{16}$$

Paris law defines the fatigue crack growth rate as a function of the amplitude of stress intensity factor:

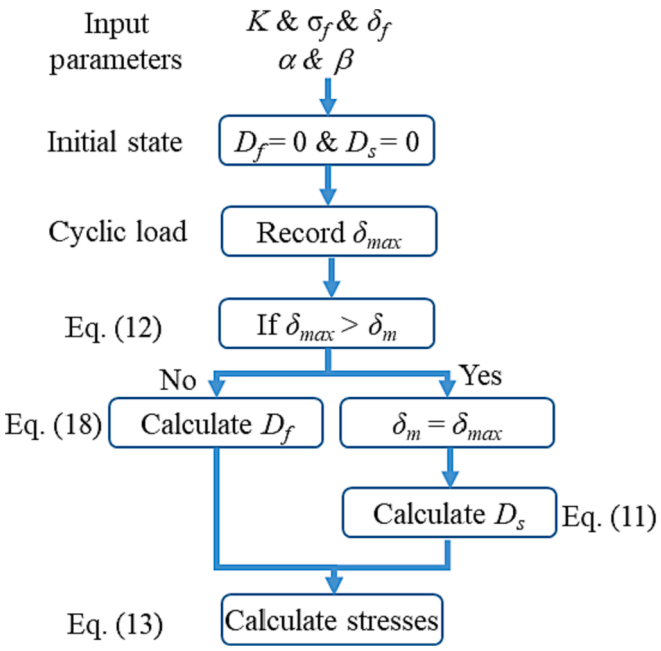

Fig. 3. Flowchart for the implementation of the cyclic CZM into VUMAT.

$$\frac{da}{dN} = C(\Delta K)^m \tag{17}$$

where a is the crack length and da/dN is the fatigue crack growth in a cycle; ΔK is the range of stress intensity factor in a cycle; C and m are material coefficients obtained from experiments.

Inspired by the form of Paris law, we propose to use a power function to describe the relationship between fatigue damage increment and stress state as follows:

$$\frac{dD_f}{dN} = \alpha\left[\frac{\sigma_{max}}{(1-D_f)\sigma_f}\right]^{\beta} \tag{18}$$

where α and β are the material parameters that need to be determined based on experimental S–N curve.

Eq. (18) can also be written as follows:

$$(1-D_f)^{\beta} dD_f = \alpha\left(\frac{\sigma_{max}}{\sigma_f}\right)^{\beta} dN \tag{19}$$

The integral of Eq. (19) on two sides can be written as follows:

$$-\frac{(1-D_f)^{1+\beta}}{1+\beta} = \alpha\left(\frac{\sigma_{max}}{\sigma_f}\right)^{\beta} N + \text{constant} \tag{20}$$

Due to the monotonic failure occurs at the first cycle, i.e., (N = 1, $\frac{\sigma_{max}}{\sigma_f}$=1 and $D_f = 0$), the constant can be obtained and Eq. (20) can be expressed as follows:

$$-\frac{(1-D_f)^{1+\beta}}{1+\beta} = \alpha\left(\frac{\sigma_{max}}{\sigma_f}\right)^{\beta} N - \alpha - \frac{1}{1+\beta} \tag{21}$$

For a typical S–N curve established from experiments under constant amplitudes, unstable failure occurs at fatigue life N_f. Therefore, the residual strength for the unstable failure is same as the stress amplitude, i.e.,

$$(1-D_{fmax})\sigma_f = \sigma_{max} \tag{22}$$

where D_{fmax} is the maximum fatigue damage value.

Eq. (22) can also be written as follows:

$$D_{fmax} = 1 - S \tag{23}$$

where S is the stress level σ_{max}/σ_f.

Therefore, Eq. (21) can be expressed based on S–N curve as follows:

$$-\frac{S^{1+\beta}}{1+\beta} = \alpha S^{\beta} N_f - \alpha - \frac{1}{1+\beta} \tag{24}$$

Eq. (24) can also be written as follows:

$$N_f = \frac{1 - S^{1+\beta} + \alpha(1+\beta)}{\alpha S^{\beta}(1+\beta)} \tag{25}$$

3.2. Determination of fatigue parameters and discussion

In the S–N curve or fatigue tests, a number of data (S_i,N_{fi}) are given. Therefore, the S–N data (S_i,N_{fi}) can be used to determine the parameters α and β by least-squares fitting of Eq. (25). It should be mentioned that, the value of N_{fi} may vary from one to hundreds of thousands for low-cycle fatigue, which makes the variance extremely unequal [4]. A weighted least-squares method is required to avoid overfitting around the data with a large value of N_{fi}. The weighted least-squares fitting can be described as follows:

$$SSR = \sum w_i\left(N_{fi} - \widehat{N_{fi}}\right)^2 \tag{26}$$

where SSR is the summed square of residuals; $\widehat{N_{fi}}$ is the fitted results. w_i are the weights which is defined as follows in this study:

$$w_i = \left(\frac{N_{fmax}}{N_{fi}}\right)^2 \tag{27}$$

where N_{fmax} is the maximum number of cycles to failure in fatigue tests.

A worked example for determining the parameters α and β based on experimental data is given in Appendix.

4. Implementation and testing

4.1. Implementation and verification

The developed cyclic CZM with nonlinear fatigue damage model is implemented into ABAQUS by a VUMAT subroutine. The VUMAT is called by ABAQUS explicit solver for quasi-static loading problems. Fig. 3 illustrates the flowchart for the calculation of the VUMAT. First, basic parameters in a monotonic CZM (i.e., penalty stiffness, strength and failure displacement) and fatigue parameters (α and β) are set as input parameters. At the initial states, the static and fatigue damage values are both zero. Within a loading cycle, the maximum displacement and stress are recorded to calculate the fatigue damage and static damage. If the maximum displacement is larger than the historic maximum displacement corresponding to static damage, the static damage occurs; otherwise, fatigue damage increment is calculated. Further, the stresses are updated according to the Eq. (13). The VUMAT will be called in every numerical increment and cycle until the loading is finished or the model is failed.

A worked example of three-point bending beam of concrete is used to demonstrate the application of the developed numerical method. Fig. 4 shows the mesh and dimensions of the worked example. The dimensions of the 2D plane strain model are the same as those in [13]. Zero-thickness cohesive elements are inserted into the potential cracking path. The length of cohesive element is 2 mm which is sufficiently small for modelling the fracture process zone in concrete. It should be mentioned that the minimum size of element which is the shortest edge for bulk element or the length of cohesive element directly determines the numerical efficiency for ABAQUS explicit solver. The smaller the minimum size is, the longer time the computation will take. There are 9,858 bulk elements and 64 cohesive elements in the model. It should be

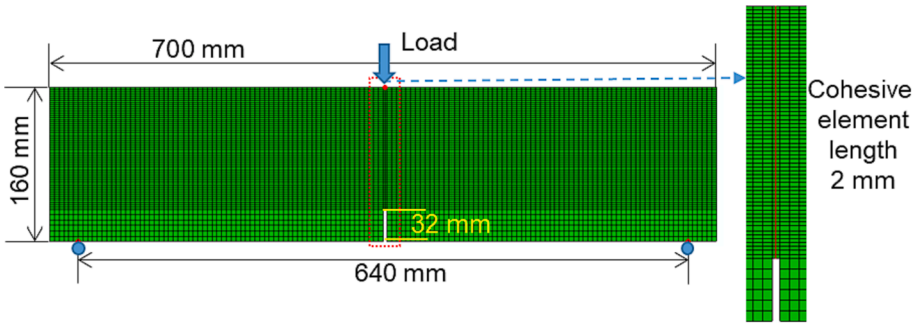

Fig. 4. Discrete model for the worked example.

Table 1
Parameters in the worked example [13].

Stress level (S)	0.90	0.85	0.80	0.75	0.70
Number of cycles to failure (N_f)	181	698	3346	18,091	94,074
Determined fatigue parameters	$\alpha = 0.003225$ & $\beta = 25.03$				
Young's modulus	34.61 GPa				
Poisson's ratio	0.21				
Penalty stiffness	10,000 GPa				
Tensile strength	2.34 MPa				
Fracture energy	129.4 N/m				

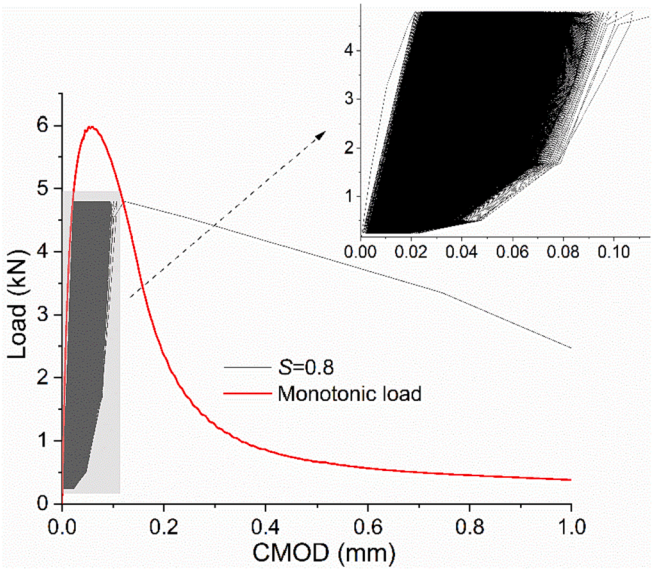

Fig. 5. Load-CMOD curves for the monotonic and cyclic loads.

mentioned that given the calculation of cyclic damage in the meantime of static fracture damage cycle by cycle, it is extremely time-consuming even for a model with 64 cohesive elements. A typical simulation for 1 cycle takes about 1 min by parallel computation using 16 Intel Core i9-10885H CPUs @2.4 GHz. The S–N data from experiments [13] are used for the determination of fatigue parameters. Table 1 shows the S–N data from [13] and other input parameters in the worked example. It should be noted that the flexure strength from the three-point bending beam tests is normally 1.4–2.8 times larger than direct tensile strength [50]. Therefore, the tensile strength used in the model is set as 70% of the measured strength from the three-point bending beam tests [13] for comparison purpose. The monotonic loading controlled by displacement is first applied to obtain the static peak load of the beam. Then a certain percentage of the static peak load is cyclically applied to the beam for fatigue modelling. To meet the requirements for quasi-static modelling and avoid dynamic fluctuations, the monotonic loading time is set as 0.2

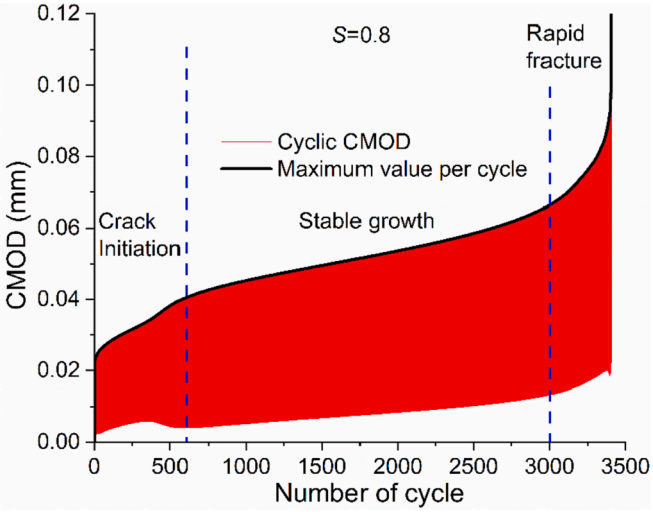

Fig. 6. CMOD development as a function of cycle number.

s. The loading rate for cyclic and monotonic loading are set as the same.

The Load-Crack Mouth Opening Displacement (P-CMOD) curve is a key output for three-point bending beam test. Fig. 5 illustrates the P-CMOD curves for monotonic and cyclic loading. The cyclic load varies from 5% to 80% of the static peak load. It can be seen that, for monotonic loading, the load first increases and then decreases after the peak load 6.01 kN. Although the stress-displacement curve prior to the peak stress is linear in the cyclic CZM, the overall load-CMOD curve of the beam is nonlinear. This is because the cohesive stresses are non-uniformly distributed in the fracture process zone which leads to the overall nonlinear behaviour. For cyclic loading, the load and CMOD cyclically increase and decrease. However, the irreversible displacement gradually accumulates until the CMOD is close to the monotonic envelope. Subsequently, the load-bearing capacity of the beam is reached and unstable failure occurs. The P-CMOD curve generally translates towards the right and the cyclic P-CMOD curve is sparse-dense-sparse along the x-axis with the cycle increasing. It is interesting to find that, within the first cycle, the unloading curve significantly differs with the loading curve and does not return to the origin. Fig. 6 shows the CMOD development as a function of the cycle number. It can be seen that, the maximum CMOD first rapidly increases before cycle 600, then almost linearly increases between 600 and 3000 cycles, and rapidly increases after cycle 3000. The unstable failure occurs at cycle 3408. The stable growth cycles account for 70% of the entire fatigue life. Therefore, the CMOD development can be divided into three stages: crack initiation, stable growth and rapid fracture. The cracking mechanisms behind the three stages will be discussed in the next section. This CMOD development trend has a very good agreement with numerous experimental results on fatigue crack growth [5,45,51].

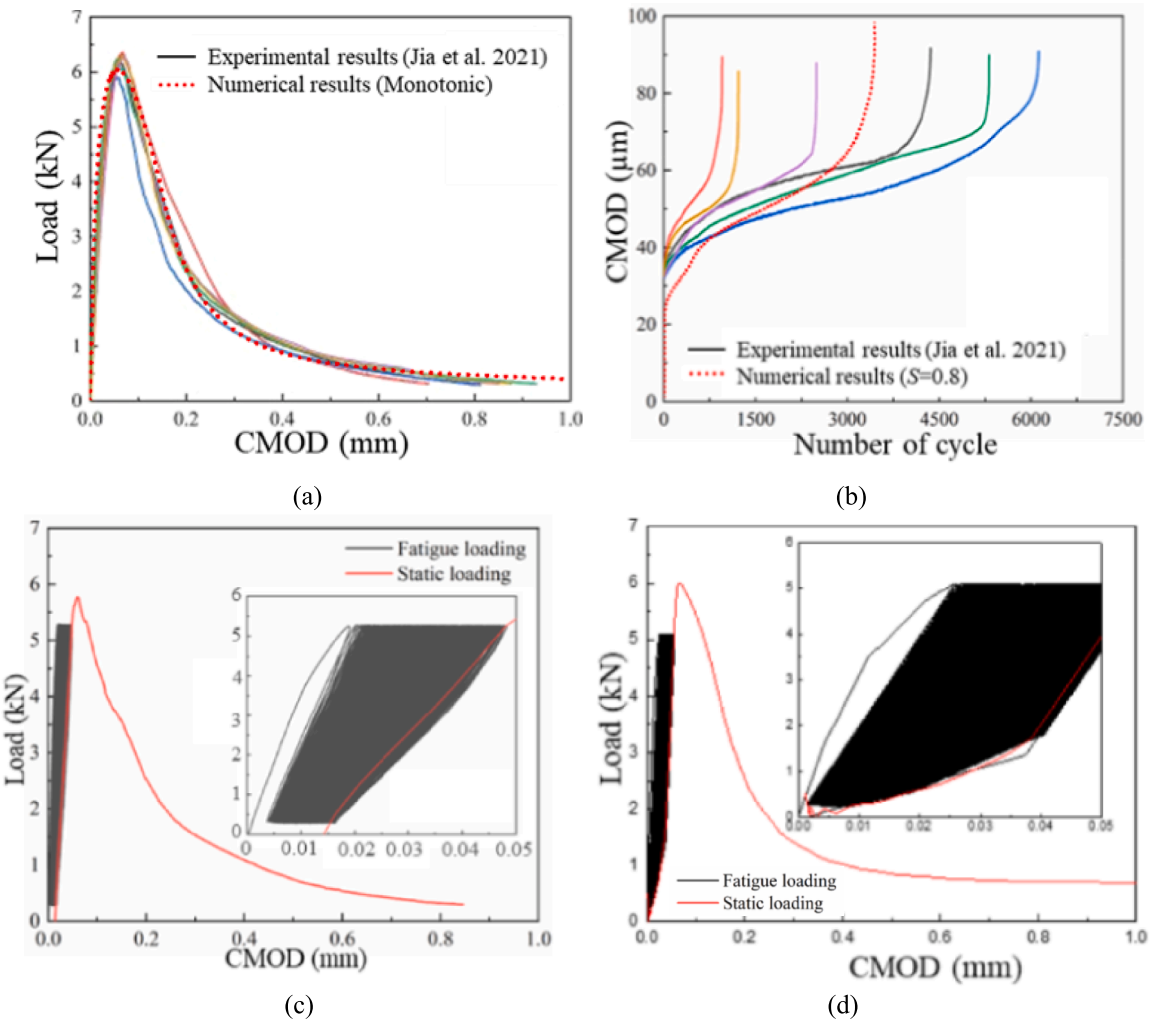

Fig. 7. Verification of the numerical model with experimental results: (a) monotonic stress-displacement curve; (b) CMOD development as a function of cycle number; (c) load-CMOD curve from cyclic-static loading from experiments; (d) load-CMOD curve from cyclic-static loading from simulations.

Fig. 7 illustrates the verification of the developed numerical method with experimental results [13]. Fig. 7a shows the P-CMOD curve for monotonic loading. It can be seen that, the P-CMOD curve is consistent with that from experimental results. The peak load from numerical modelling is 6.01 kN and the average value of peak loads from six testing specimens is 6.21 kN. Fig. 7b compares the CMOD developments from numerical model and experiments. It can be seen that, the CMOD development of concrete under the same fatigue load significantly varies amongst samples. The highly scattering experimental data is mainly caused by the heterogeneity of concrete. The randomness of aggregates leads to an uncertainty of static strength. Moreover, the stress level is based on the mean strength of six specimens. Therefore, the uncertainty of fatigue failure is exaggerated because the realistic stress level for each specimen is not exactly the same. For both experimental and numerical results, the CMOD values first rapidly increase then linearly increases and finally rapidly increase until failure, corresponding to the three stages of the cracking development. The CMOD curve from the numerical model has a good agreement with those from experimental results. Fig. 7c-d are P-CMOD curves for combined fatigue and static loading which applies 85% of monotonic peak load to the concrete beam for 70% of fatigue life and then applies monotonic load until failure. The fatigue life for stress level 0.85 is 588 which is obtained by numerical modelling prior to the combined fatigue-static modelling. It can be seen that, the P-CMOD curve gradually translates towards the right until it reaches the monotonic fracture failure envelop. For the monotonic loading after fatigue, the P-CMOD curve does not start at the origin and an irreversible displacement exists. There is a fluctuation of P-CMOD curve in the numerical results. This is because the resistance is zero in the irreversible displacement while the monotonic displacement loading causes dynamic fluctuations in ABAQUS explicit solver. For combined fatigue-static loading, the P-CMOD curve from the numerical model has also a good agreement with that from experimental results. Therefore, the developed cyclic CZM, nonlinear fatigue damage model and numerical method are reliable and accurate for low-cycle fatigue crack growth modelling of quasi-brittle materials.

4.2. *Fatigue crack mechanisms*

It is of significance to investigate the fatigue cracking mechanism behind the three-point bending beam fatigue tests. The worked example with the cyclic stress level $S = 0.8$ is used to discuss the fatigue crack mechanisms. Fig. 8 illustrates the typical local in-situ fatigue behaviour of the first cohesive element at the notch tip. Fig. 8a shows the stress-displacement curves at the notch tip and the monotonic stress-displacement curve is added for reference. During the first cycle, the static damage has already occurred because the stress at the notch tip exceeds the tensile strength of cohesive element. This static damage is the reason for the significant difference between the loading and unloading P-CMOD curves within the first cycle. However, the load-bearing capacity still exists at the post-peak stage for quasi-brittle

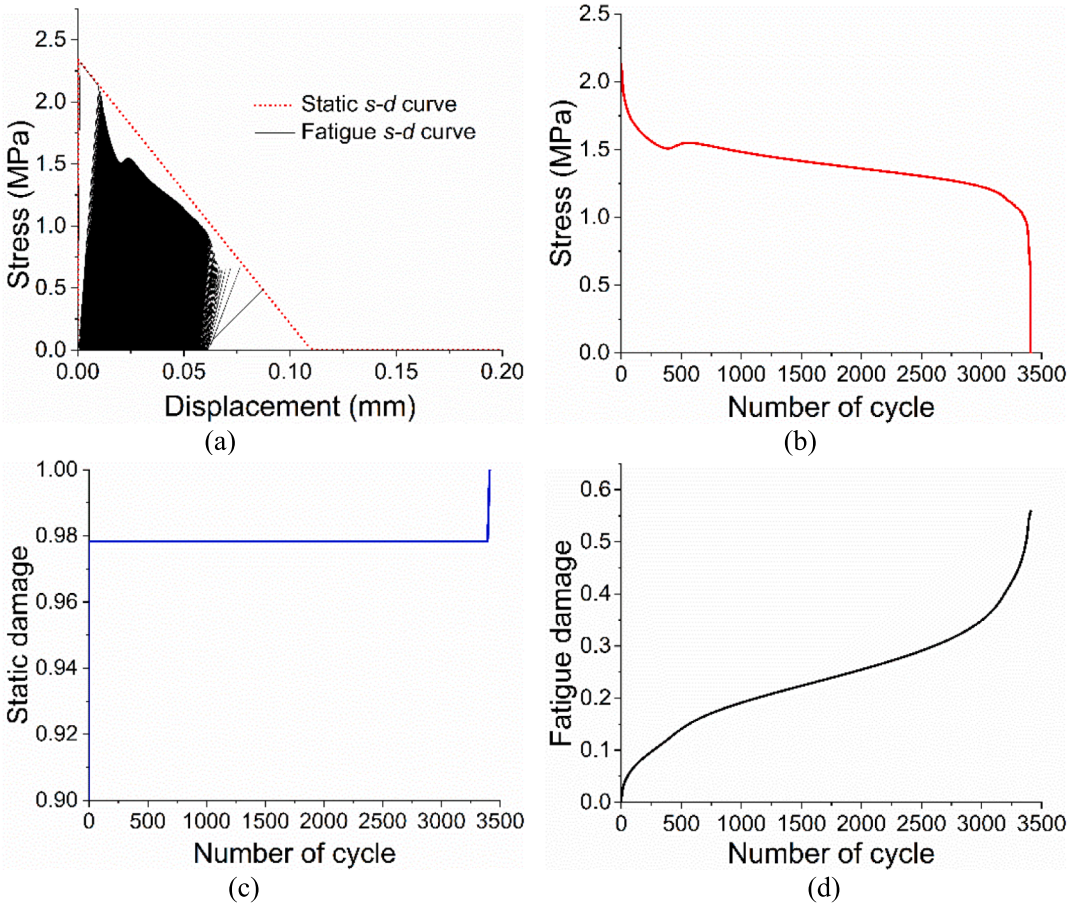

Fig. 8. Fatigue damage behaviour of the first cohesive element at the notch tip: (a) stress-displacement curve with static curve as a reference; (b) maximum stress development; (c) static damage evolution; (d) fatigue damage evolution.

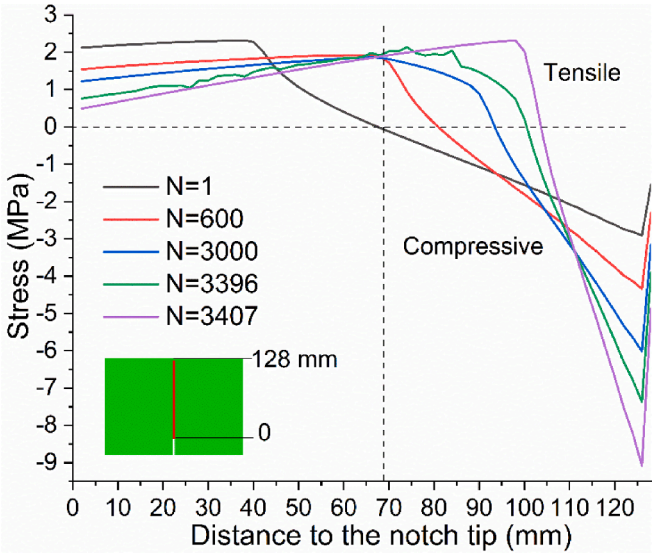

Fig. 9. Normal stress distribution of the cohesive elements at different cycles.

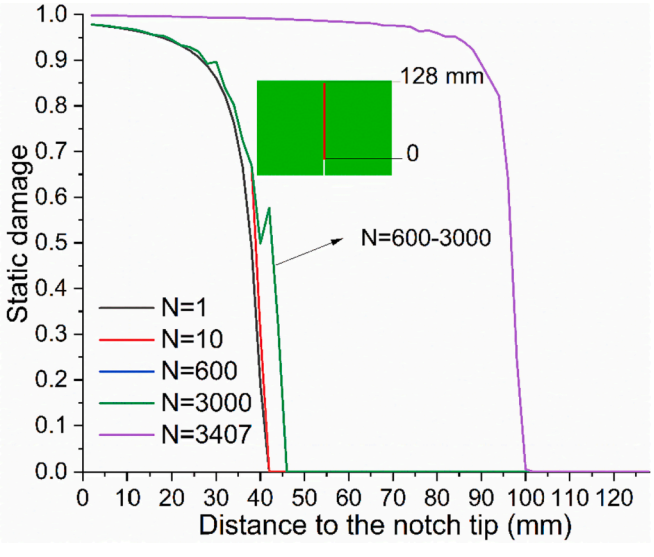

Fig. 10. Static damage evolution of the cohesive elements at different cycles.

materials oriented from the fracture process zone. For next loading cycles, the displacement does not exceed the historic maximum displacement corresponding to static damage so fatigue damage accumulates. Although the external loads are the same for each cycle, the local in-situ stress at the notch tip gradually decreases due to degradation (see Fig. 8b). Fig. 8c shows the static damage suddenly increases at the first cycle but keeps the same until close to failure. Fig. 8d shows the fatigue damage evolution at the notch tip. It can be seen that the fatigue damage first increases fast, then gradually develops and finally reaches catastrophic growth. The fatigue damage evolution is dependent on the ratio of the cyclic maximum stress to the residual strength. Therefore, fatigue life prediction based on the overall external loading amplitudes is

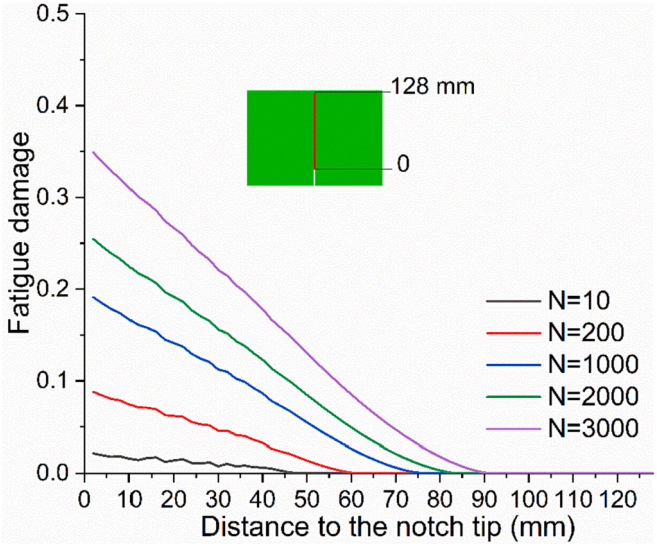

Fig. 11. Fatigue damage evolution of the cohesive elements at different cycles.

inaccurate. The prediction of structural fatigue cracking should consider the in-situ stress and fatigue damage.

Fig. 9 illustrates the normal stress distributions of the cohesive elements at the maximum load in different cycles. There is a significant compressive zone close to the top-loading point, which is a shortcoming for three-point beam bending tests to determine the tensile fracture properties. After the first loading cycle, there is a high tensile stress zone near the notch tip. At the crack initiation stage from cycle 1 to 600, the length of high tensile stress zone increases from 40 to 68 mm while the maximum stress decreases from around 2.1 MPa to 1.7 MPa. From cycle 600 to 3000 which is the stable growth stage of CMOD, the peak stress stays at the location of 68 mm while the stress from 0 to 68 mm gradually decreases. Therefore, the zone with a length of 0–68 mm from the notch tip is the main bearing zone for stable crack growth stage. For rapid fracture stage after cycle 3000, the peak stress point gradually moves towards the top-loading point. At the penultimate cycle 3407 in Fig. 9, the stress at the notch tip has still not reached zero, which means that the true crack does not form until the unstable failure.

Fig. 10 shows the static damage distributions of cohesive elements for different cycles. It can be seen that, at the first cycle, the static damage zone is from 0 to 42 mm. From 1 to 600 cycles (i.e., the crack initiation stage), the static damage zone increases from 42 mm to 46 mm and the static damage increases for most cohesive elements. However, for the stable growth stage (600–3000 cycles), the static damage never changes. After 3000 cycles, the static damage rapidly increases in both spatial range and magnitude value. Fig. 11 shows the fatigue damage distribution of cohesive elements for different cycles. It can be found that, the length of fatigue damage zone gradually increases with the cycle increasing and the fatigue damage values also gradually increase. The closer the cohesive element is to the notch tip, the fatigue damage value is generally larger. At the stable growth stage from cycle 600 to 3000, the fatigue zone length grows from 68 mm to 90 mm, which is slower than that for crack initiation and rapid fracture stages. Therefore, it can be summarised that: (1) the crack initiation stage involves the combined static and fatigue damage; (2) the stable growth stage is controlled by the fatigue damage accumulation; and (3) the rapid fracture is also a combined static and fatigue damage process but dominated by static damage. For structural fatigue failure of quasi-brittle materials,

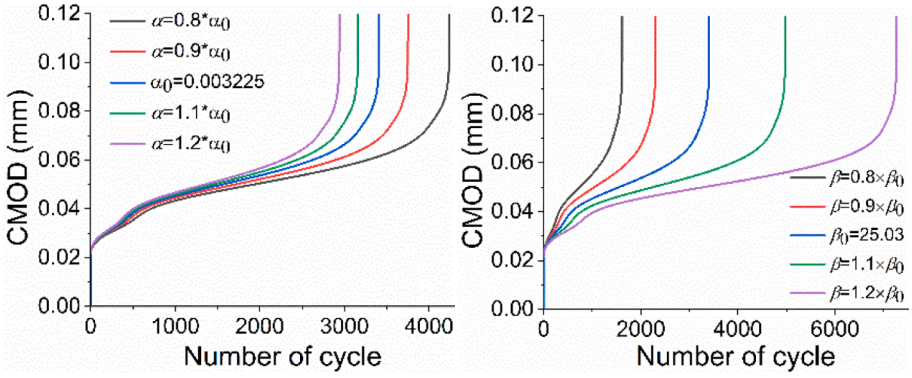

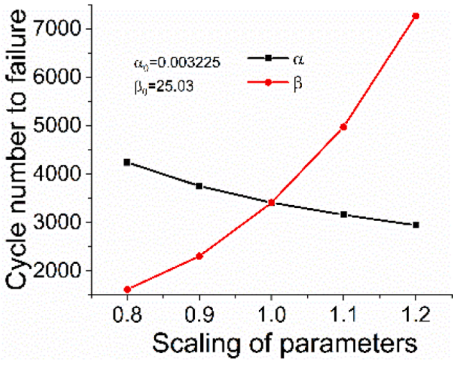

Fig. 12. Effect of fatigue parameters on the fatigue failure: (a) CMOD development affected by α; (b) CMOD development affected by β; (c) sensitivity of α and β on the number of failure cycle.

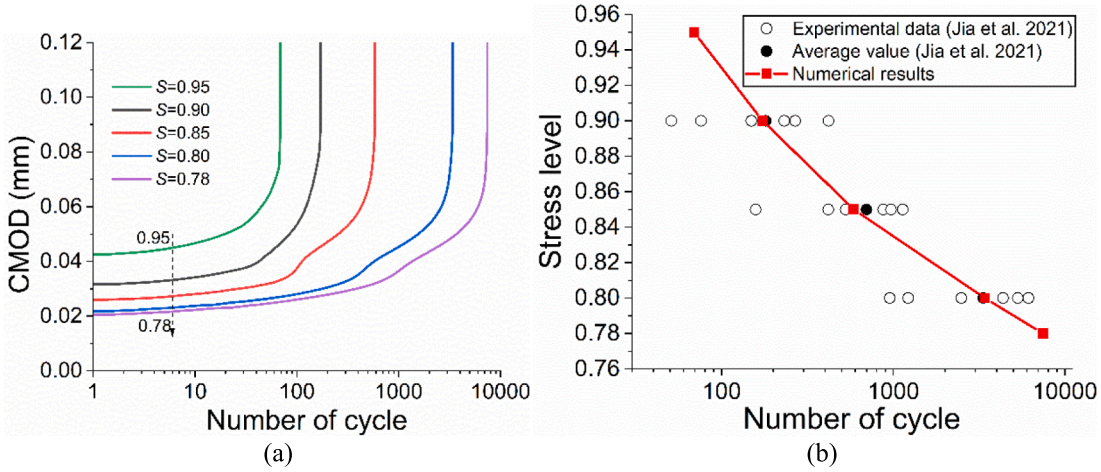

Fig. 13. Effect of stress level on the fatigue failure: (a) CMOD development; (b) S–N curve.

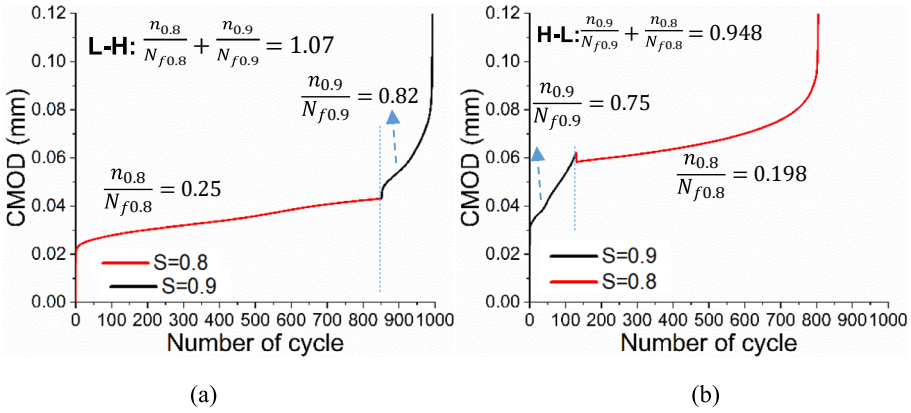

Fig. 14. Effect of loading sequence on the CMOD developments: (a) low to high amplitudes; (b) high to low amplitudes.

Table 2
Values of S–N data from experiments [52].

Stress level (S)	0.85	0.75	0.65
Number of cycles to failure (N_f)	296	6307	75,232

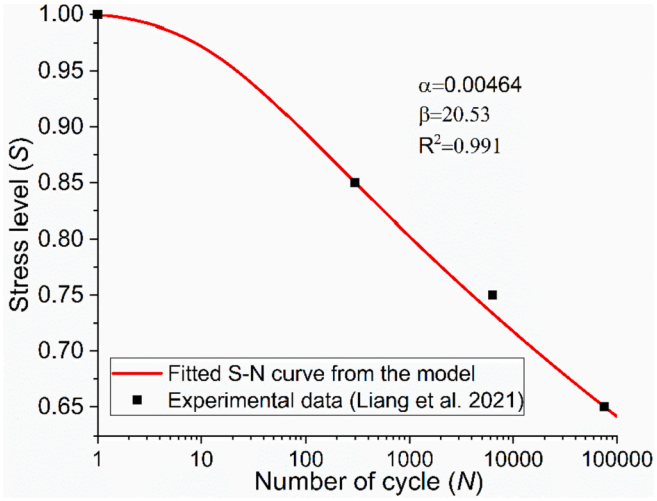

Fig. 15. S–N curve from the nonlinear damage model and the experimental data.

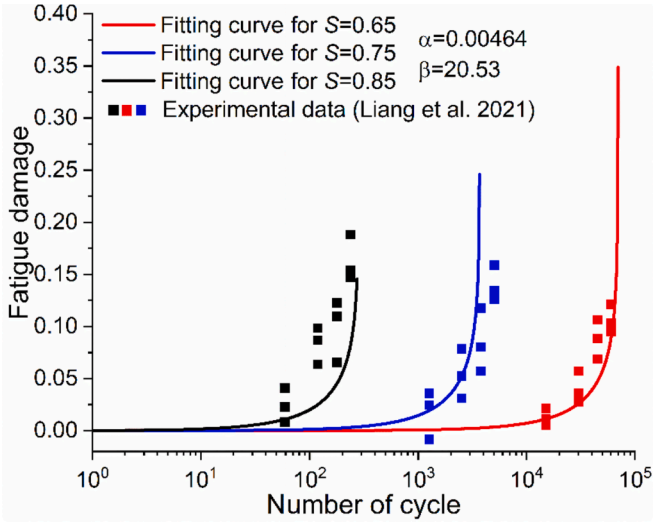

Fig. 16. Comparison of the fatigue damage evolution from the model and experimental data.

the static damage and fracture process zone still play a significant part.

4.3. Parametric studies

The parameters α and β in the proposed nonlinear fatigue model are obtained from fatigue S–N data. The parameters vary with different materials and experimental data. It is necessary to investigate the effects of fatigue parameters on the fatigue cracking. Fig. 12 illustrates the effects of fatigue parameters on the fatigue failure for cyclic stress level 0.8. It can be seen that, the larger the parameter α is, the faster the CMOD develops. The effect of parameter α on the stable growth stage is more significant than that on crack initiation and rapid fracture stages. This is because the stable growth stage is controlled by the fatigue damage. The larger the parameter β is, the slower the CMOD progresses. When α increases from $0.8\alpha_0$ to $1.2\alpha_0$, the fatigue life is decreased by 30% from 4239 to 2943 cycles, in an almost linear manner. When β increases from $0.8\beta_0$ to $1.2\beta_0$, the fatigue life exponentially rises by 350% from 1618 to 7263 cycles. It can be postulated that the fatigue life is more sensitive to the parameter β.

Fig. 13 shows the effects of cyclic stress level on the CMOD development and fatigue life. First of all, larger stress level leads to larger CMOD growth during the first cycle. This is because a larger stress level induces a larger static damage at the first cycle. Moreover, the cyclic stress level significantly affects the fatigue life. The S–N curve from numerical results shows that, when the stress level decreases from 0.95 to 0.78, the fatigue life increases from 69 to 7435 cycles. The predicted fatigue life from numerical simulations has a good agreement with that obtained from experimental results.

Fig. 14 illustrates the effects of loading sequences on the fatigue failure of concrete beam. $N_{f0.9} = 588$ and $N_{f0.8} = 3408$ are the fatigue life for stress level 0.9 and 0.8, respectively. For low to high loading amplitudes, the cyclic loading with stress level 0.8 is first applied on the beam for 25% of $N_{f0.8}$ then the cyclic loading with stress level 0.9 is applied until failure. It can be seen that, the CMOD first grows fast then almost linearly increases at the stress level 0.8. Once the stress level is changed from 0.8 to 0.9, there is a fast CMOD growth following a sudden CMOD growth. The sudden growth of CMOD is because the improved load increases the opening of cohesive elements. The fast growth is caused by the improvement of stress level. Moreover, the ratio of residual fatigue life to whole fatigue life for stress level 0.9 is 0.82 thus the sum of fatigue life fractions is 1.07. For a linear fatigue damage described by Miner's rule [41], the sum of fatigue life percentages should be 1. Therefore, for low to high amplitudes, the predicted life from the numerical results is longer than Miner's prediction. For high to low loading amplitudes, the cyclic loading with stress level 0.9 is first applied on the beam for 75% of $N_{f0.9}$ then the cyclic loading with stress level 0.8 is applied until fatigue failure. It can be seen that, the CMOD first fast increases at the stress level 0.9. When the stress level is changed from 0.9 to 0.8, the CMOD curve suddenly decreases due to the reduced load shortens the opening displacement of cohesive elements. Then a stable growth of CMOD exists until rapid fracture and failure. Therefore, once the static damage is formed by a high stress level, the CMOD development becomes stable under a low stress level. Moreover, the sum of fatigue life fraction is 0.948 which is smaller than 1. Therefore, for high to low amplitudes, the predicted life from the numerical results is shorter than Miner's prediction. The effects of loading sequences on the sum of fatigue life fractions from the numerical results are consistent with conclusions from experimental results, i.e., in relation to the Miner's rule, high to low loading scenario leads to the fatigue life reduction while the low to high loading sequence results in an extension [52].

5. Conclusions

In this paper, a cyclic cohesive zone model is developed for low-cycle fatigue of quasi-brittle materials. In the cyclic CZM, the fatigue damage accounts for irreversible displacement accumulation and the static damage controls the stiffness degradation. A nonlinear fatigue damage model is proposed for calculating fatigue damage in the cyclic CZM. The fatigue damage parameters are determined based only on experimental S–N data and the fatigue damage evolution derived from the fatigue model is in a good agreement with that from experimental results. Further, the developed cyclic CZM is implemented into ABAQUS by a VUMAT subroutine. A worked example for monotonic and cyclic loading of three-point bending concrete beam is presented to demonstrate the application of the developed numerical method. The numerical results have a good agreement with the experimental results. Moreover, the fatigue crack mechanisms are discussed through stress and damage analyses. Finally, comprehensive parametric studies are carried out to investigate the effects of fatigue parameter, stress level and loading sequence on the fatigue failure. It has been found that, there are three stages for the development of CMOD, i.e., crack initiation, stable growth and rapid fracture which are caused by combined static and fatigue damage, fatigue damage, and combined static and fatigue damage dominated by static damage, respectively. At the fatigue controlled stable growth stage, the peak tensile stress along the potential crack path stays at a fixed location and static damage along the potential crack path never increases. The fatigue life is more sensitive to the fatigue parameter β than α. With the parameter β increasing, the fatigue life exponentially increases. The stress level also significantly affects the fatigue life. When the stress level decreases from 0.95 to 0.78, the fatigue life increases from 69 to 7435. Moreover, for low to high amplitude loading sequence, the predicted fatigue life from the numerical model is longer than that from Miner's rule which is based on a linear fatigue damage law. But for high to low loading amplitudes, the predicted fatigue life from the numerical model is shorter than Miner's prediction.

Declaration of Competing Interest

The authors declare that they have no known competing financial interests or personal relationships that could have appeared to influence the work reported in this paper.

Data availability

Data will be made available on request.

Acknowledgement

Financial support from the UK Engineering and Physical Sciences Research Council (EPSRC) for the project "Smart Pulses for Subsurface Engineering" with grant number (EP/S005560/1) is gratefully acknowledged.

Appendix: Worked example for the determination of fatigue parameters

A worked example for concrete fatigue cracking is presented to demonstrate the proposed method for the determination of fatigue parameters. Liang et al. [52] obtained S–N data for concrete by three-point beam bending tests under cyclic loads with different loading amplitude (see Table 2). Moreover, fatigue-induced strength reductions were obtained through combined fatigue-static tests that first applied cyclic loading for 20%, 40%, 60% and 80% of fatigue life respectively then monotonic loads were applied to measure the residual strengths of concrete [52]. Therefore, the fatigue damage evolution was determined based on the residual strengths in Liang's tests [52]. The parameters α and β from the fitting results are 0.00464 and 20.53, respectively. Fig. 15 illustrates the S–N curve from the fatigue model with fitted parameters and experimental data. The scatter points are from the experiment and the red line is from the developed model. It can be seen that, the S–N curve from the fatigue model has a good agreement with the

experimental data [52]. The coefficient of determination R^2 is 0.991. It is interesting to find that, the S–N curve from the fatigue model is nonlinear at the stress level higher than 0.95, which is consistent with experimental results [53]. Fig. 16 shows the comparison of fatigue damage evolution from the proposed fatigue model and experimental data [52]. It can be found that, the fatigue damage evolution from the fatigue model has also a good agreement with those from experiments. The fatigue damage is very small at the first 20–40% of the fatigue life due to the loading amplitude is relatively much smaller than the residual strength. With the fatigue damage increasing and the residual strength gradually decreasing, the fatigue damage increment becomes larger and larger until a sudden unstable failure. Therefore, the proposed nonlinear fatigue damage model is practically significant and its parameters are easy to be determined based only on experimental S–N data. The S–N curve from the fatigue model is nonlinear and accurate for low-cycle fatigue life prediction. Moreover, the nonlinear fatigue damage evolution can also be well described by the fatigue model which can be used in the cyclic cohesive zone model. It should be mentioned that, more data on concrete fatigue cracking are required to determine the fatigue parameters for statistical validation with higher accuracy.

References

[1] Z.P. Bazant, J.-L. Le, Probabilistic Mechanics of Quasibrittle Structures: Strength, Lifetime, and Size Effect, Cambridge University Press, Cambridge, 2017.
[2] C. Sun, G. Li, M.E. Gomah, J. Xu, H. Rong, Experimental investigation on the nanoindentation viscoelastic constitutive model of quartz and kaolinite in mudstone, Int. J. Coal Sci. Technol. 8 (5) (2021) 925–937.
[3] X. Chen, J. Bu, X. Fan, J. Lu, L. Xu, Effect of loading frequency and stress level on low cycle fatigue behavior of plain concrete in direct tension, Constr. Build. Mater. 133 (2017) 367–375.
[4] X. Chen, J. Bu, L. Xu, Experimental Study on Cyclic Tensile Behavior of Concrete under High Stress Level, ACI Mater. J. 114 (5) (2017).
[5] N.K. Banjara, K. Ramanjaneyulu, Experimental Investigations and Numerical Simulations on the Flexural Fatigue Behavior of Plain and Fiber-Reinforced Concrete, J. Mater. Civ. Eng. 30 (8) (2018).
[6] Y. Ji, L. Zhuang, W. Wu, H. Hofmann, A. Zang, G. Zimmermann, Cyclic Water Injection Potentially Mitigates Seismic Risks by Promoting Slow and Stable Slip of a Natural Fracture in Granite, Rock Mech. Rock Eng. (2021).
[7] X. Xi, S. Yang, C.I. McDermott, Z.K. Shipton, A. Fraser-Harris, K. Edlmann, Modelling Rock Fracture Induced By Hydraulic Pulses, Rock Mech. Rock Eng. (2021).
[8] W. Liu, L. Zhang, N. Luo, Elastic modulus evolution of rocks under heating–cooling cycles, Sci. Rep. 10 (1) (2020) 13835.
[9] T. Saksala, R. Kouhia, A. Mardoukhi, M. Hokka, Thermal jet drilling of granite rock: a numerical 3D finite-element study, Philos. Trans. Royal Soc. A: Mathem. Phys. Eng. Sci. 379 (2196) (2021) 20200128.
[10] W. Schütz, A history of fatigue, Eng. Fract. Mech. 54 (2) (1996) 263–300.
[11] J. Schijve, Fatigue of structures and materials in the 20th century and the state of the art, Int. J. Fatigue 25 (8) (2003) 679–702.
[12] B. Cerfontaine, F. Collin, Cyclic and Fatigue Behaviour of Rock Materials: Review, Interpretation and Research Perspectives, Rock Mech. Rock Eng. 51 (2) (2017) 391–414.
[13] M. Jia, Z. Wu, R.C. Yu, X. Zhang, Residual fracture energy of concrete suffering from fatigue loading, Eng. Fract. Mech. 255 (2021).
[14] N. Erarslan, H. Alehossein, D.J. Williams, Tensile Fracture Strength of Brisbane Tuff by Static and Cyclic Loading Tests, Rock Mech. Rock Eng. 47 (4) (2013) 1135–1151.
[15] N. Pugno, M. Ciavarella, P. Cornetti, A. Carpinteri, A generalized Paris' law for fatigue crack growth, J. Mech. Phys. Solids 54 (7) (2006) 1333–1349.
[16] P. Paris, F. Erdogan, A critical analysis of crack propagation laws, (1963).
[17] S. Nojavan, D. Schesser, Q.D. Yang, An in situ fatigue-CZM for unified crack initiation and propagation in composites under cyclic loading, Compos. Struct. 146 (2016) 34–49.
[18] K. Kirane, Z.P. Bažant, Microplane damage model for fatigue of quasibrittle materials: Sub-critical crack growth, lifetime and residual strength, Int. J. Fatigue 70 (2015) 93–105.
[19] A. Hillerborg, M. Modeer, P.E. Petersson, Analysis of crack formation and crack growth in concrete by means of fracture mechanics and finite elements, Cem. Concr. Res. 6 (6) (1976) 773–781.
[20] Z. Yang, W. Ren, R. Sharma, S. McDonald, M. Mostafavi, Y. Vertyagina, T. J. Marrow, In-situ X-ray computed tomography characterisation of 3D fracture evolution and image-based numerical homogenisation of concrete, Cem. Concr. Compos. 75 (2017) 74–83.
[21] Z. Yang, X. Frank Xu, A heterogeneous cohesive model for quasi-brittle materials considering spatially varying random fracture properties, Comput. Method. Appl. M. 197 (45–48) (2008) 4027–4039.
[22] W. Ren, Z. Yang, R. Sharma, C. Zhang, P.J. Withers, Two-dimensional X-ray CT image based meso-scale fracture modelling of concrete, Eng. Fract. Mech. 133 (2015) 24–39.
[23] Z.-J. Yang, B.-B. Li, J.-Y. Wu, X-ray computed tomography images based phase-field modeling of mesoscopic failure in concrete, Eng. Fract. Mech. 208 (2019) 151–170.
[24] S. Yang, K. Li, C.-Q. Li, Analytical model for non-uniform corrosion-induced concrete cracking, Mag. Concrete. Res. (2017) 1–10.
[25] P. Guo, J. Gu, Y. Su, J. Wang, Z. Ding, Effect of cyclic wetting–drying on tensile mechanical behavior and microstructure of clay-bearing sandstone, Int. J. Coal Sci. Technol. 8 (5) (2021) 956–968.
[26] Y. Chen, J. Zuo, D. Liu, Y. Li, Z. Wang, Experimental and numerical study of coal-rock bimaterial composite bodies under triaxial compression, Int. J. Coal Sci. Technol. 8 (5) (2021) 908–924.
[27] S. Yang, X. Xi, K. Li, C.-Q. Li, Numerical Modeling of Nonuniform Corrosion-Induced Concrete Crack Width, J. Struct. Eng. 144 (8) (2018) 04018120.
[28] B. Yang, S. Mall, K. Ravi-Chandar, A cohesive zone model for fatigue crack growth in quasibrittle materials, Int. J. Solids. Struct. 38 (22–23) (2001) 3927–3944.
[29] M. Kuna, S. Roth, General remarks on cyclic cohesive zone models, Int. J. Fracture. 196 (1–2) (2016) 147–167.
[30] S. Roth, G. Hütter, M. Kuna, Simulation of fatigue crack growth with a cyclic cohesive zone model, Int. J. Fracture. 188 (1) (2014) 23–45.
[31] H. Khoramishad, A.D. Crocombe, K.B. Katnam, I.A. Ashcroft, Predicting fatigue damage in adhesively bonded joints using a cohesive zone model, Int. J. Fatigue 32 (7) (2010) 1146–1158.
[32] H. Khoramishad, A.D. Crocombe, K.B. Katnam, I.A. Ashcroft, A generalised damage model for constant amplitude fatigue loading of adhesively bonded joints, Int. J. Adhes. Adhes. 30 (6) (2010) 513–521.
[33] H. Khoramishad, A.D. Crocombe, K.B. Katnam, I.A. Ashcroft, Fatigue damage modelling of adhesively bonded joints under variable amplitude loading using a cohesive zone model, Eng. Fract. Mech. 78 (18) (2011) 3212–3225.
[34] I. Benedetti, V. Gulizzi, A grain-scale model for high-cycle fatigue degradation in polycrystalline materials, Int. J. Fatigue 116 (2018) 90–105.
[35] K.L. Roe, T. Siegmund, An irreversible cohesive zone model for interface fatigue crack growth simulation, Eng. Fract. Mech. 70 (2) (2003) 209–232.
[36] A. Needleman, An analysis of decohesion along an imperfect interface, Int. J. Fracture. 42 (1) (1990) 21–40.
[37] A. Skar, P.N. Poulsen, J.F. Olesen, A simple model for fatigue crack growth in concrete applied to a hinge beam model, Eng. Fract. Mech. 181 (2017) 38–51.
[38] A. Skar, P.N. Poulsen, J.F. Olesen, General cracked-hinge model for simulation of low-cycle damage in cemented beams on soil, Eng. Fract. Mech. 175 (2017) 324–338.
[39] F. Parrinello, V. Gulizzi, I. Benedetti, A computational framework for low-cycle fatigue in polycrystalline materials, Comput. Method. Appl. M. 383 (2021), 113898.
[40] F. Parrinello, I. Benedetti, A coupled plasticity-damage cohesive-frictional interface for low-cycle fatigue analysis, Int. J. Mech. Sci. 224 (2022), 107298.
[41] M.A. Miner, Cumulative damage in fatigue, (1945).
[42] A. Aeran, S.C. Siriwardane, O. Mikkelsen, I. Langen, A new nonlinear fatigue damage model based only on S-N curve parameters, Int. J. Fatigue 103 (2017) 327–341.
[43] D.-G. Shang, W.-X. Yao, A nonlinear damage cumulative model for uniaxial fatigue, Int. J. Fatigue 21 (2) (1999) 187–194.
[44] A. Turon, J. Costa, P.P. Camanho, C.G. Dávila, Simulation of delamination in composites under high-cycle fatigue, Compos. A Appl. Sci. Manuf. 38 (11) (2007) 2270–2282.
[45] S. Nojavan, D. Schesser, Q.D. Yang, A two-dimensional in situ fatigue cohesive zone model for crack propagation in composites under cyclic loading, Int. J. Fatigue 82 (2016) 449–461.
[46] X. Xi, Z.K. Shipton, J.E. Kendrick, A. Fraser-Harris, J. Mouli-Castillo, K. Edlmann, C.I. McDermott, S. Yang, Mixed-Mode Fracture Modelling of the Near-Wellbore Interaction Between Hydraulic Fracture and Natural Fracture, Rock Mech. Rock Eng. (2022).
[47] X. Xi, S. Yang, Z. Shipton, M. Cai, Modelling the near-wellbore rock fracture tortuosity: Role of casing-cement-rock well system, perforation and in-situ stress, Int. J. Rock Mech. Min. Sci. 157 (2022), 105182.
[48] X. Xi, S. Yang, C.-Q. Li, M. Cai, X. Hu, Z.K. Shipton, Meso-scale mixed-mode fracture modelling of reinforced concrete structures subjected to non-uniform corrosion, Eng. Fract. Mech. 199 (2018) 114–130.
[49] J. Lemaitre, A. Plumtree, Application of damage concepts to predict creep-fatigue failures, (1979).
[50] Z. Huang, Y. Zhang, Y. Li, D. Zhang, T. Yang, Z. Sui, Determining Tensile Strength of Rock by the Direct Tensile, Brazilian Splitting, and Three-Point Bending Methods: A Comparative Study, Adv. Civil Eng. 2021 (2021) 5519230.
[51] K. Kirane, Z.P. Bažant, Size effect in Paris law and fatigue lifetimes for quasibrittle materials: Modified theory, experiments and micro-modeling, Int. J. Fatigue 83 (2016) 209–220.
[52] L. Lei, S. Xingang, C. Yunhua, W. Lefan, Y. Xiangcheng, A new fatigue damage model for pavement concrete beams bearing multi-level bending loads, PLoS ONE 16 (8) (2021), e0255048.
[53] I. Burhan, H.S. Kim, S-N Curve Models for Composite Materials Characterisation: An Evaluative Review, J. Compos. Sci. 2 (3) (2018) 38.
[54] K. Park, H. Choi, G.H. Paulino, Assessment of cohesive traction-separation relationships in ABAQUS: A comparative study, Mech. Res. Commun. 78 (2016) 71–78.

[55] X. Xi, S. Yang, C.-Q. Li, A non-uniform corrosion model and meso-scale fracture modelling of concrete, Cem. Concr. Res. 108 (2018) 87–102.
[56] B. Gong, M. Paggi, A. Carpinteri, A cohesive crack model coupled with damage for interface fatigue problems, Int. J. Fracture. 173 (2) (2012) 91–104.
[57] C.G. Dávila, From S-N to the Paris law with a new mixed-mode cohesive fatigue model for delamination in composites, Theor. Appl. Fract. Mech. 106 (2020).
[58] H. Li, H. Yuan, X. Li, Assessment of low cycle fatigue crack growth under mixed-mode loading conditions by using a cohesive zone model, Int. J. Fatigue 75 (2015) 39–50.
[59] S. del Busto, C. Betegón, E. Martínez-Pañeda, A cohesive zone framework for environmentally assisted fatigue, Eng. Fract. Mech. 185 (2017) 210–226.